Expertise
and insight
for the future

Harri Karppi

Motion control for CBCT gantry

Metropolia University of Applied Sciences

Master of Engineering

Information Technology

Master's Thesis

1 November 2019

PREFACE

This thesis is final work on my Master's studies in the field of information technology and has also been a part of my work in Planmeca. The thesis was undertaken as a part of a new CBCT development and building process. In devices like CBCT, a lot of effort and knowledge are put together for achieving a functioning device. And being part of this process has taught me a lot. The motivation for writing this thesis was to document the building process of motion control in detail.

I would like to thank my colleagues and my supervisor, Design Manager, Mr. Juha Kolehmainen, for his support and feedback. And thanks for Senior software designer Mr. Pertti Hokkanen, for providing his expertise and ideas related to this work.

And finally, I would like to thank my family for supporting me throughout the thesis writing process and studies.

Helsinki, 25.10.2019
Harri Karppi

Author Title Number of Pages Date	Harri Karppi Motion control for CBCT gantry 44 pages + 4 appendices 1 Nov 2019
Degree	Master of Engineering
Degree Programme	Information Technology
Instructor(s)	Juha Kolehmainen, Design Manager Matti Fischer, Principal Lecturer

This thesis is a study on developing a motion controller for an X-ray imaging arm based on the requirements specification. A proof-of-concept motion control is designed and tested. The main goal was to correspond with the requirement specification in parts concerning the motion control. This study was done by identification, build, data collection, analysis, and results method.

The identification was made at a high level by studying the requirements specification, the X-ray imaging device constructions, and the motion control technologies. Once the identification was made, a prototype motion control hardware was selected, designed, implemented, and tested. After the motion control testing, the results were analyzed and compared against the requirements specification. And the future development recommendations were given. The hardware design is described in detail, but the embedded software is excluded from this thesis since the author did not do it. Only the motion control high-level description is presented.

The selected motion control technologies included two absolute position encoders, a motor driver utilizing a closed-loop vector control, and a surface-mounted permanent magnet synchronous motor. One sensor was used to provide the position feedback of the imaging arm for the motion controller. And the other sensor provided the speed and angular position of the PMSM rotor for the motor driver.

The overall result from this study was that the selected motion control technologies were adequate for meeting the requirements specification. And some future enhancements should be considered regarding motion control velocity profiles and motor sizing.

Keywords	PMSM, Motor control, Motion control

Contents

List of Abbreviations

ACIM	AC Induction Motor
AC	Alternative Current
CBCT	Cone Beam Computed Tomography
CAD/CAM	Computer-Aided Design / Computer-Aided Manufacture
CT	Computed Tomography
CAN	Controller Area Network
DFT	Design For Testing
ECAD	Electronic Computer-Aided Design
EMI	Electro-Magnetic Interference
FPGA	Field Programmable Grid Array
FOC	Field Oriented Control
ICS	Isolated Current Sensor
IGBT	Insulated Gate Bipolar Transistor
IM	Induction Motor
IPMSM	Internal Permanent Magnet Synchronous Motor
Mosfet	Metal oxide semiconductor field-effect transistor
MCPU	Master Central Processing Unit
MCU	Micro Controller Unit
PCB	Printed Circuit Board
PE	Protective Earth
PFC	Power Factor Correction
PID	Proportional Integral Derivative controller
PMSM	Permanent Magnet Synchronous Motor
PWM	Pulse Width Modulation
SDK	Software Development Kit
SPI	Serial Peripheral Interface
SSI	Standard Serial Interface
SVPWM	Space Vector Pulse Width Modulation
SVC	Sensored Vector Control
SCARA	Selective Compliant Articulated Robot Arm
VFD	Variable Frequency Drive

1 Introduction

This study was done for Planmeca Oy, which is one of the leading dental equipment manufacturers in the world. The product portfolio of Planmeca Oy consists of digital dental units, 2D and 3D X-ray imaging devices, CAD/CAM products, and supporting software solutions. The annual turnover of the Planmeca group in 2018 was 746 MEUR. With the number of employees globally, nearly 2800. The Planmeca Oy is family-owned and founded in 1971. The headquarters, along with the product development and manufacturing premises, are all located in Helsinki, Finland. [1]

The subject of this study is a selection, building, and verification of a motion control system for a cone-beam computed tomography device imaging arm. The study was done by identification, build, data collection, analysis, and results method.

The main components of the motion control system are the motor, the motor controller, the embedded software, and the mechanical parts in which it is installed. This study evaluates the different motion control technologies, their properties, and describes the initial selection for the design. For the evaluation of the drive system performance, a prototype drive system is implemented and tested. The primary goal of this study was to develop a motion control system that fulfills the requirements specification of the device.

2 Theoretical Background

2.1 Construction of CT Imaging Devices

The computed tomography imaging device utilizes X-rays, detectors, and an image presentation device for producing an X-ray image for diagnostic purposes.

The basic construction of the CT X-ray imaging system is shown in Figure 1. The imaging arm is the supporting structure for the imaging devices, which are the X-ray source and an X-ray detector. This configuration creates an isocenter point and a rotational path for the source and detector. In a computed tomography scan, a set of X-ray measurements, are taken from the object from different angles. The actual X-ray image is a grayscale measurement of the X-ray beams and their attenuation between the path from the source to a detector [2]. In CBCT imaging, usually, a flat panel detector (FPD) is used to capture the X-ray image from the region of interest (ROI). A data acquisition module (DAQ) transfers the images to a reconstruction computer, which creates the 3D volume by utilizing a filtered back-projection algorithm.

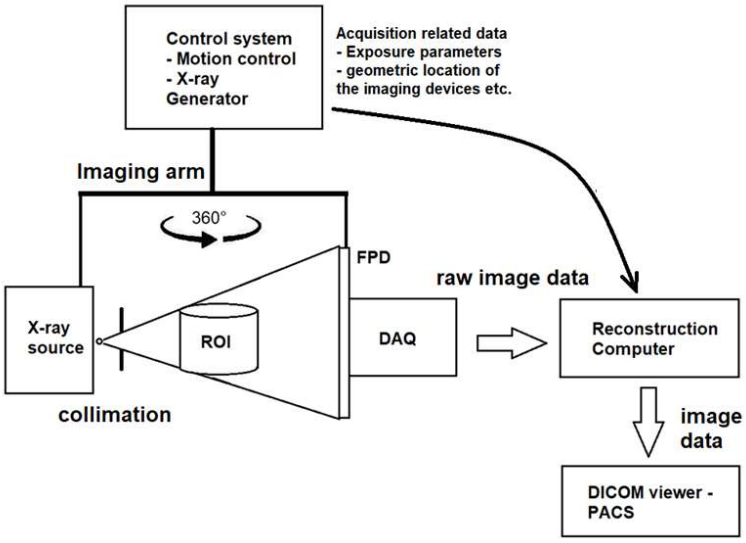

Figure 1. A simplified CBCT imaging system description in C-arm configuration

The resulting X-ray digital images are stored in DICOM format (standard Digital Imaging and Communications in Medicine format). The acquired X-ray images can be viewed and archived with several available free or commercial software.

The clinical image viewer and archiving systems are referred to as PACS (Picture Archiving and Communication System)

The CBCT imaging differs from the CT by the acquisition speed, size, and shape of the irradiated area. In a traditional computed tomography device. The x-ray beam is narrow, or fan-like, compared to the conical shape of CBCT (Figure 2). The cone beam shape can capture a larger volume in a single revolution of the imaging arms, depending on the detector size.

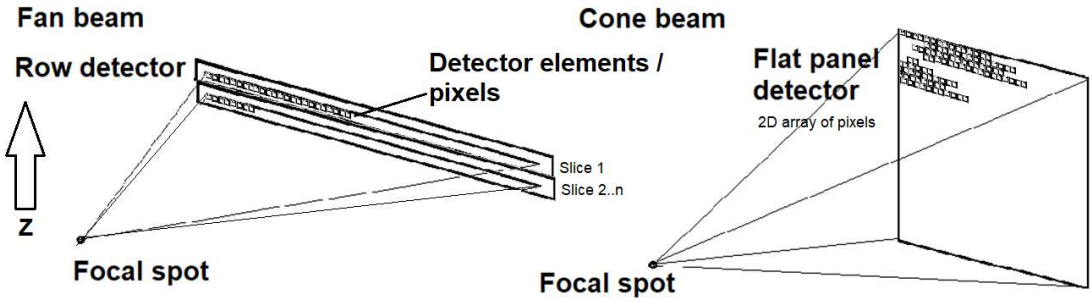

Figure 2. The difference between a fan and cone-beam CT

In a CBCT volume acquisition, the detector and X-ray source are rotating partial or a full revolution and simultaneously acquiring a set of several hundred X-ray measurements from the region of interest (ROI). The imaging arm motion is relatively slow. The image acquisition usually lasts 10-30 seconds and rotating 210° – 360°. From the acquired x-rays, a 3D volume can then be reconstructed by using a filtered back-projection algorithm.

In a 3D reconstruction, the scanned raw data is corrected, calculated, and presented as a 3D matrix of voxels in the field of view. Figure 3. shows a CBCT reconstruction.

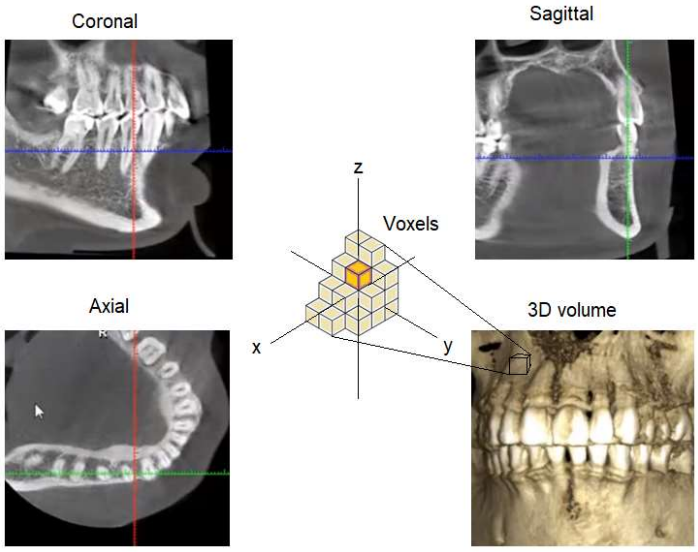

Figure 3. A CBCT reconstruction viewed and edited from Planmeca Romexis viewer and presenting the concept of voxel

Each voxel is assigned an HU grey value depending on the attenuation it represents. This stack can be shown in 3D or along different planes for visualization in 2D. A standard tri-planar view includes axial, sagittal, and coronal slices, as well as the reconstructed volume.

The image reconstruction is computationally complex. For example, in CBCT, a raw image consists of more than a million pixels, with each pixel assigned for 12 to 16-bit of data (the grey value). And a single reconstruction dataset can include over 500 projections. The actual reconstruction time depends on several parameters, which are numbers of projections, the field of view, voxel size, processing speed, data throughput, computational performance, and the reconstruction algorithm in use. The reconstruction is usually done in less a minute.

In an X-ray device, the X-ray source is a high voltage component where the X-rays are generated. The X-ray generator controls the voltage and current between the anode and cathode of an X-ray high vacuum tube. The X-ray image contrast and grayscale are altered by controlling the properties of the emitted X-rays from the X-ray tube by adjusting the voltage and current parameters and with the use of beam filtration.

There are two types of X-ray source operating modes — the continuous and pulsed exposure mode. In the pulsed mode, the X-ray source voltage is switched on and off

between the detector acquisition and readout. The pulsed mode is used for minimizing the patient dose and is a conventional technique in flat panel detector-based CBCT imaging, where the detector readout cycle is around 50Hz. In CT devices, also in CBCT panoramic exposures, the detector row readout can be >1 kHz, requiring continuous exposure.

The different imaging arm configurations are used in different applications, see figure 4, such as the C-arm configurations, which are usually found in dental CBCT and mobile surgery X-ray devices. The gantry or O-arm construction offers a more robust mechanical design. The O-arm is found in CT scanners, but can also be found in some CBCT imaging devices. The selective compliant articulated robot arms (SCARA) can be found in dental CBCTs and surgery room robotic X-ray machines.

Figure 4. Different CT imaging devices. 1. Planmeca Viso (SCARA and C-arm), 2. Medtronic O-arm, 3. Philips Pulsera 3D (C-arm) 4. Toshiba Aquilion 64 (Gantry with slip rings)

The CT scanner gantry or O-arm is a rotating frame construction utilizing a slip ring that enables free rotation of the imaging devices. The motion control for a gantry rotation of CT is usually implemented with a direct/linear drive system or with a belt-driven configuration [3]. Moreover, the rotational speeds of 180 ms or less can be achieved with modern high-speed CT devices [4].

2.2 Motion Control

The motion control system is used for controlling the mechanical loads, position, velocity, torque, acceleration, and deceleration. The elements on which the motion control system is composed, are the Human-machine interface, motion controller, motor controller, the motor, transmission mechanics, and feedback [5]. The performance of a servo system is characterized as the system step response and the accuracy of control. Figure 5 shows the concept of closed-loop motion control.

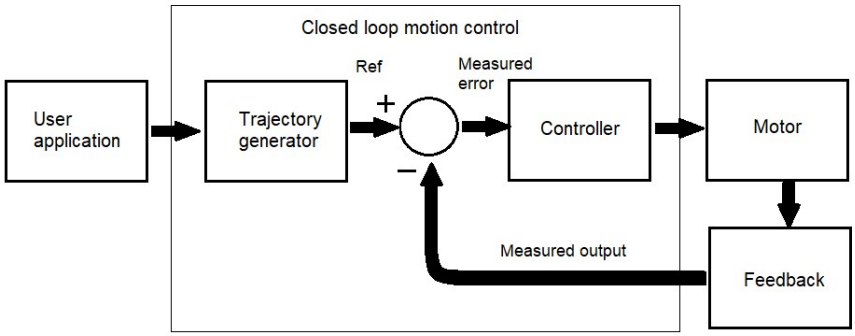

Figure 5. The concept of closed-loop motion control

The user application, for example, the selected imaging modality, sets the limits in which the motion is executed. The trajectory generator assembles the reference speed plot for the controller to be executed. During the motion, feedback is used for monitoring. The controller compares and adjusts against the actual position to the desired set point.

Depending on the trajectory or velocity profile, the motion is divided into three stages, which are the acceleration, velocity plot, and deceleration.

There are two typically used velocity profiles, the trapezoidal and S-curve, shown in Figure 6. The trapezoidal speed profile is straightforward to implement since the acceleration and deceleration stages are executed at a constant rate. The trapezoidal velocity profile contains discontinuities in corners of acceleration and deceleration stages. This

causes jerks in the system and might cause mechanical vibrations [5]. The S-curve velocity profile rounds the sharp corners of the velocity profile, providing a smooth transition between the stages.

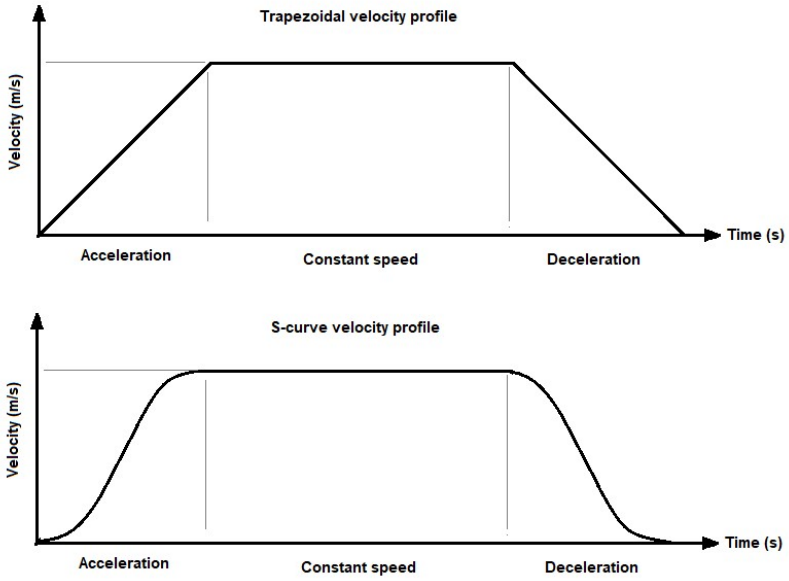

Figure 6. Trapezoidal and S-curve velocity profiles

For enhancing the servo system step response and stability, a velocity feedforward function can be introduced. The input velocity is fed forward directly to the velocity loop. When rapid changes occur on the velocity profile, they are instantly transferred to the velocity control loop [5]. Figure 7. illustrates the velocity feedforward motion control scheme. The feedforward control is used to remove a setpoint and other disturbances before getting into the controller [6].

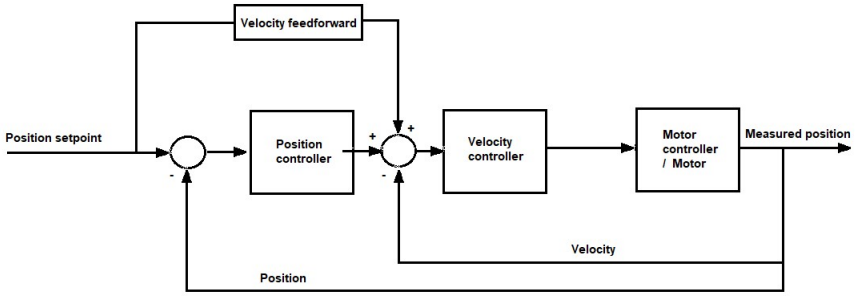

Figure 7. Velocity feedforward motion control

The motion control of the imaging device contributes to the image quality at the acquisition phase. The repeatability of the imaging trajectories should be highly accurate and vibration-free. The motion control of the x-ray devices imaging arm plays a significant role in a chain of the successful image acquisition process.

The motion controller adjusts the movement of the X-ray source and the detector, which are rotating around the region of interest. In an imaging system, a poorly performing motion control system can result in degraded image quality, limit the use of the device, or exhibit as a premature system failure. To avoid the unwanted properties or malfunctioning, proper evaluation and study of the drive system are essential for the successful end-product.

The motion control for a gantry rotation of CT is usually implemented with a direct/linear drive system or with a belt-driven configuration. It also has a different set of requirements regarding motion control, comparing to a CBCT. The image acquisition process is a straightforward constant speed operation. So the requirement for the motion control is to maintain a constant speed of the gantry rotation. This kind of drive performance can be achieved with an asynchronous induction motor, a rotational position encoder for feedback, and with the use of a variable frequency drive.

In a C-Arm construction, motion control is servo control. C-arm and SCARA need precise motion control for accurate movement of the imaging devices. The accurate motion control is also used to replicate the programmed imaging trajectories, which is essential for the geometric calibrations to work.

2.3 Electric Motors

The electric motors can broadly be classified into two categories on the basis of how they produce torque electromechanically or by variable reluctance.

In the electromechanical method, the motoring is the interaction of two magnetic fields, one generated by the stator and other by the rotor. Interacting together, they generate electromagnetic torque when trying to align the fields.

In the variable reluctance motors, the motion is generated by the result of variable reluctance between the rotor and stator. The stator is a part of the magnetic circuit aligning into a minimum reluctance position between the energized coils [5.]. There is a broad range of different motors in the market and competing switching and control topologies. Here are presented some most common types and their properties.

AC Induction motor (IM, ACIM)

The asynchronous induction motor is the most common type of electric motors in industrial applications. The ACIM utilizes the squirrel cage construction or windings in the rotor. The ACIM is a robust and straightforward construction that can easily last a lifetime of the end-product. Asynchronous means that the mechanical speed of the rotor is different from the speed of the revolving magnetic field; the rotor has a slip. So the slip induces the rotor currents. [7] The induced currents build up the rotor magnetic fields, which interact with the rotating stator field and generate the torque. The available speed range of ACIM is a function of the selected driver technology. In variable frequency drive (VFD) use, ACIM usually needs an encoder of some sort. The ACIM is not used in applications demanding high precision positioning.

Brushless DC motor (BLDC)

The BLDC is a synchronous DC motor without the mechanical commutation brushes. The commutation is produced by electronically controlling the BLDC. The BLDC requires a closed-loop controller to be operational. It can deliver high torque with a good speed response. [7] The BLDC is suitable for precise motion control, and It has a very similar construction and properties with PMSM. The back –EMF is usually trapezoidal.

Stepper Motor

Discrete steps control the stepper motor, having multiple coils organized in groups called phases. The motion is controlled by energizing each phase sequentially, taking one step at a time. Stepper motors tend to make noise when running higher speeds.

Stepper Motors are used when highly precise, and relatively slow movement is needed eq. Industrial/surgical robots. Stepper motors have a high starting torque, but the torque decreases at higher speeds.

Permanent Magnet Synchronous Motor (PMSM, IPMSM)

The PMSM is a synchronous motor type, with high efficiency and no rotor losses. The Synchronous motors rotate at the same frequency as the revolving magnetic field. The PMSM motors are usually more expensive than other types because of the use of rare-earth metals in the permanent magnets. The PMSM motors have a high zero speed torque because the rotor is permanently magnetized.

There are different configurations of placing the permanent magnets in the rotor, buried or surface mounted. The surface-mounted magnets provide a bit less vibration due to more homogenous magnetic flux distribution and sinusoidal back EMF. The buried magnet configuration allows higher operating speeds but distorts the back EMF to non-sinusoidal, causing more harmonics. [8]

Depending also on the stator winding distribution, the PMSM can be very quiet under operation by generating sinusoidal back EMF that leads to minimized torque ripple.

The PMSM has a higher torque density compared to other motors, meaning that the physical size is smaller, usually 50% compared to the same torque delivered by ACIM. The PMSM is very suitable for servo applications.

Switched reluctance motor (SRM)

The SRM is one type of stepper motor, which is usually found in high power applications. The SRM has a simple design, only iron laminates in the rotor. The SRM can achieve very high speeds, since there is no back EMF generated, and no extra energy in field weakening is needed. SRM motor has excellent energy efficiency across a wide range of loading conditions. [9]. SR motor can achieve 100 % rated torque on a standstill.

2.4 Driver circuitry

The driver is the device that powers and controls the motor through electrical circuitry. There is two feasible driver switching technologies in low-mid power range motor drives. These are IGBT and MOSFET based inverters. Many manufacturers have integrated the driver and power switching circuitry into a single package for minimizing the power losses and EMI. Selecting the switching technology IGBT or MOSFET is based on voltage and power levels and the switching frequency and losses. For low voltage high-frequency applications, the MOSFET based inverter is preferred, and when the voltage is exceeding 250 V, the use of IGBT is preferred [10].

For the Induction Motor, PMSM, and BLDC motors, high-performance motor control is characterized by smooth rotation over the entire speed range of the motor, full torque control at zero speed, fast accelerations, and decelerations and a high load transient response [11]. The most uncomplicated motor drive to implement is the brushed DC drive, where the motor speed can be controlled directly with the amplitude of the applied voltage.

For controlling an AC motor, an active electronic device is needed to form the alternative currents and frequency for the motor. The electronic device is usually called an inverter, motor controller, variable frequency drive, or a drive. It has many names, based on switching topology, the motor type being controlled and the control technique applied. Below, a basic three-phase half-bridge inverter is illustrated in Figure 8.

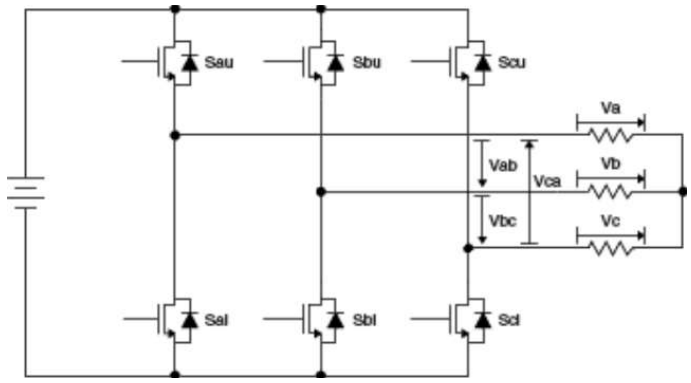

Figure 8. A three-phase three half-bridge IGBT based inverter topology [12]

For the motors, such as PMSM and BLDC, there are many different control methods available.

The control methods are used for sequencing the coil commutations to generate a directional rotation, and in where the commutation rate is proportional to motor speed.
The three central control schemes are, trapezoidal, scalar and field-oriented control

A trapezoidal control is the simplest method, referred to as 6-step control. A current path is generated between a pair of the motor windings, and a third winding is left uncoupled. The trapezoidal control generates a high torque ripple, noise, and vibration.

Scalar control, also known as the V/Hz control, supplies varying sinusoidal currents to the three-phase windings. The V/Hz operation holds the ratio of voltage and frequency constant by tracking voltage magnitude. This prevents magnetic saturation (at which a motor's rotor cannot be magnetized further, causing high currents). The voltage to be applied to coils is calculated from the applied frequency required to maintain air-gap flux. The scalar method provides easy speed control, but no direct control of motor torque. It provides weak load transient dynamics and speed response times. [13] The scalar control is the most common method for ACIM´s.

The vector control, or the field-oriented control (FOC), provides the best efficiency and performance for the drive system. The high-level FOC description is presented in Figure 9. For implementing a FOC control- the accurate knowledge of motor parameters is needed by the algorithm to execute correctly. The vector control captures the rotor position directly from the sensor or by calculating it from the motor characteristics and the current and voltage measurements, meaning the FOC can also be executed without any physical feedback sensor. This is known as the sensor-less FOC. In the sensor-less control, a state observer theory is introduced to replace the physical positioning sensors. The state observer calculates the rotor angular position by utilizing the mathematical model of the motor and measured back-EMF. The sensor-less FOC struggles in the low rpm range since the back-EMF generation is minimal. [11]

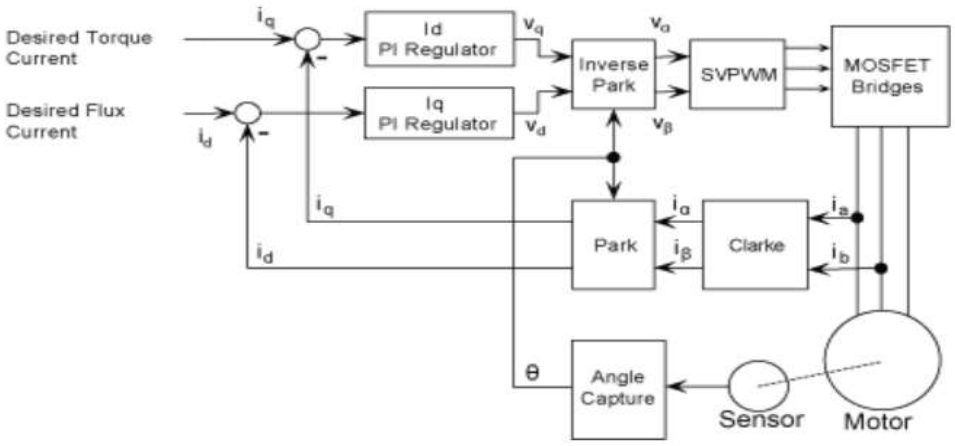

Figure 9. Field-oriented control utilizing sensor

The idea in the FOC control is to transform the three-phase system into a rotating two-coordinate system [11], which then can be easily adjusted. The control process is more like controlling a DC motor in this phase. The FOC control utilizes the Clarke and Park transformations that allow the flux (Id) and torque (Iq) components to be controlled separately in a rotating reference frame. See — figure 10 for the FOC workflow. The control loop execution rate can be in the range of > 1 kHz, meaning that the transformations and inverse transformations are executed in a fast cycle. This requires computational performance from the MCU. [12]

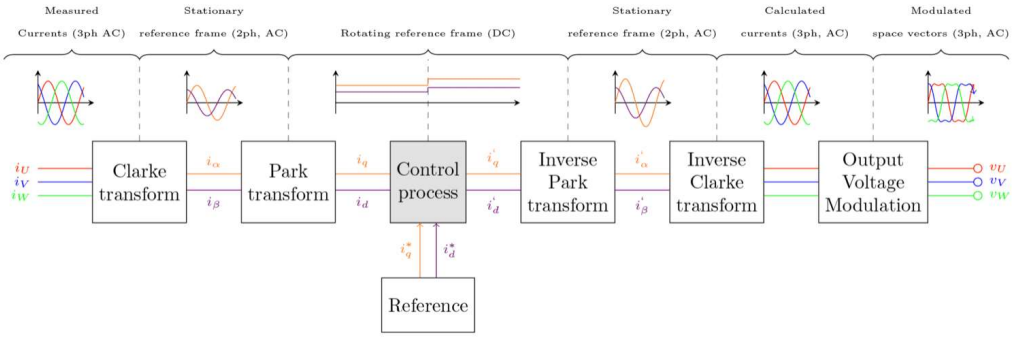

Figure 10. The workflow of the vector control [14]

In vector control, a Clarke transformation converts equal three-phase quantities into equal two-phase quadrature quantities. The second phase is Park Transformation, which

transforms a balanced two-phase orthogonal stationary system into an orthogonal rotating reference frame. The control process adjusts the flux and torque components against the referenced values, and the inverse Park and Clarke transforms are then executed. At the output stage, the space vector modulator translates the three-phase reference frame vectors into a switching sequence for controlling the three-phase half-bridges. [11]

It was described in figure 8. how the three-phase inverter is configured, and in Table 1. it is presented how the three outputs of the three-phase inverter can connect the phases of the motor to a positive or negative terminal of DC bus voltage. Since only one switch per leg must be closed, eight different states are possible. The switch states are presented in Table 1.

One common way to represent the phase voltages A, B, C is the space vector model. Figure 11. describes the space vector pulse width modulator vector diagram and how the PWM signals are controlled for achieving a rotating vector $u_{s,}$ which is the result of each phase vectors. (Fig 8 and Table 1). It is possible to associate a reference vector to each of the eight states. In order to generate a rotating field, the inverter has to be switched in six of the eight states. This mode of operation is called a six-step mode [15]. Table 1 lists the inverter six-step switch states and the phase and line-to-line voltages.

Table 1. Inverter six-step switching table [12]

Switch State			Phase Voltage (V)			Line-to-Line Voltage (V)		
S_{au}	S_{bu}	S_{cu}	V_a	V_b	V_c	V_{ab}	V_{bc}	V_{ca}
0	0	0	0	0	0	0	0	0
1	0	0	$2V_{DC}/3$	$-V_{DC}/3$	$-V_{DC}/3$	V_{DC}	0	$-V_{DC}$
1	1	0	$V_{DC}/3$	$V_{DC}/3$	$-2V_{DC}/3$	0	V_{DC}	$-V_{DC}$
0	1	0	$-V_{DC}/3$	$2V_{DC}/3$	$-V_{DC}/3$	$-V_{DC}$	V_{DC}	0
0	1	1	$-2V_{DC}/3$	$V_{DC}/3$	$V_{DC}/3$	$-V_{DC}$	0	V_{DC}
0	0	1	$-V_{DC}/3$	$-V_{DC}/3$	$2V_{DC}/3$	0	$-V_{DC}$	V_{DC}
1	0	1	$V_{DC}/3$	$-2V_{DC}/3$	$V_{DC}/3$	V_{DC}	$-V_{DC}$	0
1	1	1	0	0	0	0	0	0

The remaining two states (0,0,0 & 1,1,1) are called zero vectors because, in these states, the voltage applied in the motor windings is null due to the middle point of each leg is connected to GND or the DC bus voltage [15].

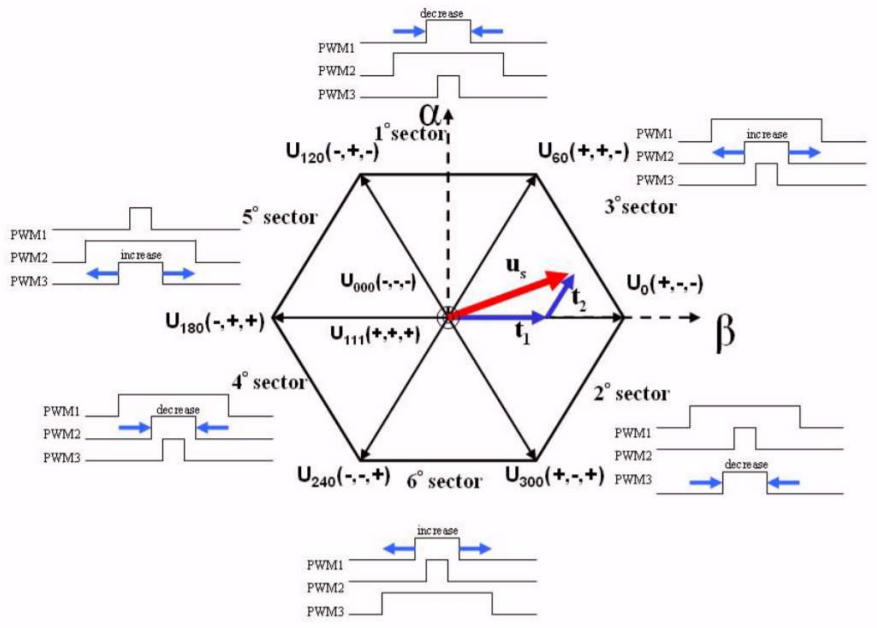

Figure 11. An SVPWM modulation vector diagram [15]

The zero vectors are located in the middle of the hexagon and can be used to regulate the amplitude of the space vector, and the angle between any two vectors is 60°.

A Voltage frequency drive can be described as an energy flow control device, providing the frequency and voltage amplitude for the use of motoring. The PMSM motor also works as a synchronous generator, reversing the energy flow. In a four-quadrant operation that is described in figure 10. The kinetic energy of the motor and the load is transformed back into electromagnetic energy in quadrants Q2 and Q4.

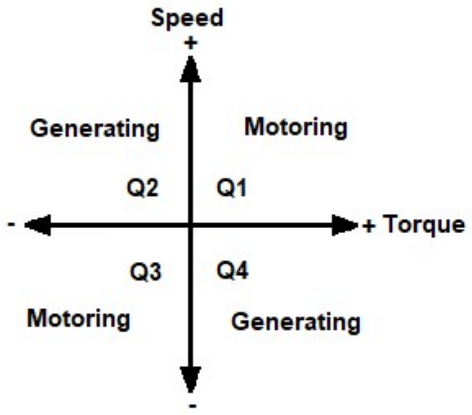

Figure 12. Four quadrant operation of electric motor

In regenerative braking or electrical braking of the PMSM, the negative q-axis current is set, and deceleration occurs. The DC-BUS capacitors absorb the energy from deceleration. When operating in the generating quadrant, care needs to be taken that the DC BUS capacitors can absorb the energy so that the generator conditions are not causing voltages above the DC BUS capacitor voltage ratings, or currents that can damage the switching components. The overvoltage condition usually occurs well above the nominal speed of the motor, which could harm the electrolytic capacitors. For preventing the DC BUS voltage rise, the energy needs to be directed. In some cases, a chopper power resistor circuit is added into DC BUS, where the energy is transformed into heat once a preset threshold limit is met. [8]

The system is equipped with a power factor correction circuitry (PFC). In generating mode where the DC BUS is absorbing, the DC bus voltage is controlled by PFC, and it will limit the energy taken from the mains. Moreover, the regenerated energy is mainly diverted into use for other devices connected to DC BUS.

The overview of different available motor technologies and control schemes suggest that for the best performing motion control option would be the synchronous PMSM motor type or BLDC utilizing closed-loop FOC control. The motor should be equipped with an angular sensor. This setup offers the most accurate speed control and zero speed maximum torque for selecting the motion control system. A stepper, BLDC, or PMSM configuration with proper feedback sensoring would provide the needed performance.
The use of sensor-less FOC offers less complicated HW design but is limited in low-speed operation.

2.5 Technical Specification

The technical requirements concerning the motion control of the imaging arm are presented in table 2. The technical requirements are extracted from the requirement specification, which can be found in appendix 1. From the requirement specification, four different movements are identified. And a relevant set of data is derived and presented in table 2. The required torques, speeds, and mass approximations for table 2. were calculated by the mechanic's team from the early CAD models. The O-arm is the gantry construction, where the imaging devices are located. A-movement is for moving the gantry construction, and the S-movement is a supplementary movement for the device.
The device movements are divided into three different categories, which are:

1. Movement during the image acquisition
2. patient positioning
3. imaging equipment offset positioning and supplementary drives

Table 2. The device motion control requirements

Category	**Movement**	**Torque / Nm**	**Speed/ cm\s**	**Force / N**	**Use during image acquisition.**
1	O-arm, gantry rotation	>6	50	-	YES
2	A-movement	>60	20	-	NO
3	S-movement	>3	10	-	NO
2	patient support	-	5	4000	NO

In category 1, motion control has the most demanding requirements since the motor is used in image acquisition. The positioning accuracy of image acquisition is set to be less than 150 µm, which requires an absolute position feedback sensor.

The imaging gantry is calculated to weigh approximately 180 kg. Moreover, the full 360° rotation time has specified to be 8 seconds or less, which includes the acceleration of the imaging gantry. This requires a motion control system of high dynamics with the ability for regenerative braking since the gantry mass distribution can be unbalanced. The motion control system should respond to load changes rapidly and preserve the accuracy of the positioning. The gear ratios are used to scale the usable motor rpm and torque to meet the requirements.

3 Motion control prototype

In this section, the construction of the motion control system for the CBCT imaging arm is described. The components and the design of motion control are presented. Also, the development tools and environments are introduced. The technology selection is made based on a literature review, studying the in-house designs and component vendors. The initial selection of driver and motor technologies are also described in this chapter. The component selection is made before the schematics are designed. This phase includes the evaluation of different component options, manufacturers, availability, lifetime estimations, and pricing. This has been outlined in this study, and only the selected components are introduced.

This section begins with the description of the motion control architecture in the prototype device and with the selection of the motor and driver framework. Also, the design workflow of the motor driver is presented.

This follows the presentation of designed motor driver technical specification, schematics, and layout in detail that is relevant for the motion control. For example, the supply voltage converters and regulators are not discussed. Also, all needed sensors and subcomponents for motion control are described.

3.1 Motion Control System Description

The gantry rotation motor was selected to be a surface mounted PMSM. The physical size, energy efficiency, minimal torque ripple, and acoustic performance were the primary selection criteria. Hanning electro werke offered a suitable motor for testing in the prototype. The motor was delivered with the following specifications:

The Hamatic compact series S56 3- phase PMSM motor.

Gearmotor S56:	synchronous version
Voltage / Frequency:	3~ 200 V
I/A, P/W:	2A, 500W
Winding size:	∅56 mm, 30 mm width
Torque:	> 6 Nm
Gear Reduction:	17,5
Speed range:	57 – 342 RPM (Motor: 1000 – 6000 RPM)

The detailed electrical motor parameters for S56 are found in Appendix 2.

In Figure 13, the motion control of the prototype device is described with the main components. The master central processing unit runs the embedded software which controls the imaging device.

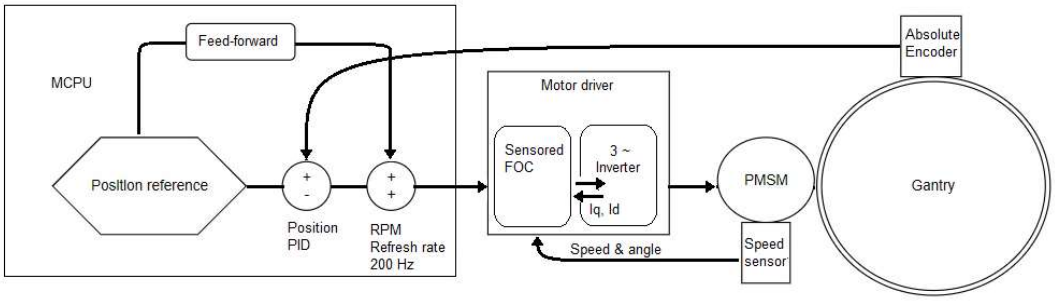

Figure 13. Prototype motion control architecture, execution rates of control loops: Pos PID 200 Hz, Speed PID 2000 Hz, current PID 16 kHz

The MCPU creates the velocity profile from the parameters received from the user interface. And as the imaging process starts, the position reference is set and transferred into

the motor driver as an rpm command through CAN-bus, this position PID rpm control loop is set to run at the rate of 200 Hz. The position PID regulator receives the absolute position data and compares and corrects the position through the rpm control loop. The absolute encoder is connected to MCPU through the standard serial interface.

The motor driver receives the CAN rpm message from MCPU and executes the received rpm command. The speed control loop is executed at a rate of 2 kHz in FOC control using the rotor angle/speed sensor, and the current PID is executed at the rate of 16 kHz.

The sensors provide feedback for the motion controller, and there are two sensors installed in the prototype device. The absolute encoder is used for the position monitoring And a speed/angular sensor for the use of a motor driver. The latter can also be used to monitor the gantry movement.

The used absolute encoder is a magnetic 16-bit rotary encoder, with a single turn accuracy of +-0.0878°. The MCPU acquires data from the sensor via the SSI interface. SSI interface cycle time is ≥ 25 µs. The maximum sampling rate is 40 kSps. And the used sensor type is UCD-S101B-1616-R06A-2RW.

The speed sensor reading the PMSM rotor speed is Giant Magneto Resistance based (GMR), which detects the orientation of the magnetic field. The magnet is positioned into a rotor shaft end.

3.2 Driver Design

For building the motor driver prototype, a specification was created. (See Appendix 3.) The demand for high performance of the motion control system suggests that the sensor vector control provides the solution for the requirements that the system has. The motor controller was decided to be implemented around the microprocessor series of STM32F4 for software development kit (SDK), software maintenance, and uniformity reasons. The power switching circuitry was selected from the same manufacturer.

The driver design was created with PADS 9.5 ECAD software. And the schematic and layout design of the driver are described in this section. The driver module design process follows a classical waterfall model.

Figure 14. The motor driver module design process

From the requirement specification, a technical specification was extracted. And based on that, all needed components are selected, and the schematic and layout design was implemented. This followed the testing phase and system integration.
The PCB layout was outlined by the cabling and mechanics. The driver PBC is designed to be enclosed and easily interchangeable.

3.2.1 Driver Layout

The driver layout was designed in a 4-layer PCB using a 70 µm copper for enhanced current carrying capability. The driver component positioning and functional blocks are described in Figure 15.

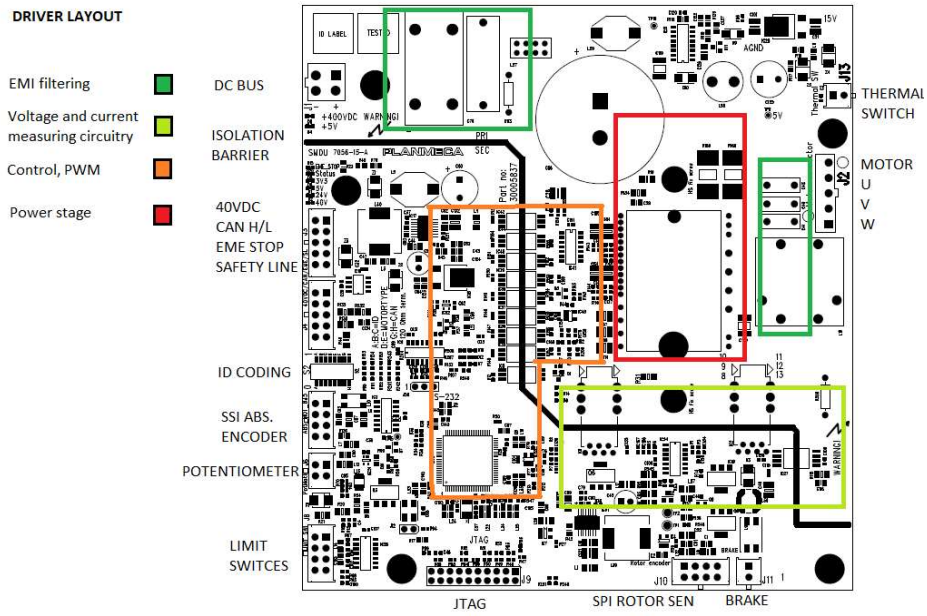

Figure 15. PCB Layout of the driver PCB

The driver is connected to the DC bus that provides the 450 VDC primary voltage for the three-phase inverter power stage (red). The EMI filtering stage consists of common-mode inductor and X-capacitors, for both input and output connections. The microcontroller generates the PWM control signals for the power stage, and the signals are optically isolated. Voltage and current measurements from the primary side are also made with isolated components.

The electrical safety of the drive system is described in figure 16.

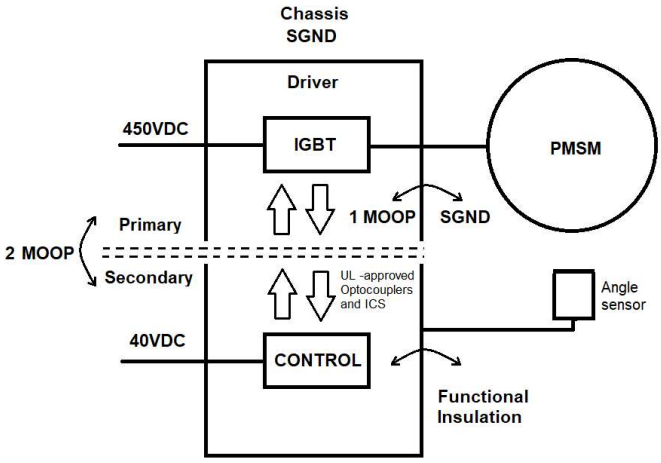

CLASSIFICATIONS	ISOLATION	CREEPAGE / CLEARANCE	INSULATION
1 x MOOP	1500 Vac	2.5 mm / 2mm	Basic
2 x MOOP	3000 Vac	5 mm / 4mm	Double
1 x MOPP	1500 Vac	4 mm / 2.5mm	Basic
2 x MOPP	4000 Vac	8 mm / 5mm	Double

Figure 16. Electrical safety requirements

The electrical safety requirements are from IEC 60601-1 3rd edition. The motion control system needs to fulfill the 2 Means Of Operator Protection isolation requirement between the primary and secondary circuits.

3.2.2 Microcontroller

In a microcontroller, a FOC algorithm controls the SVPWM modulator that provides the desired frequency and amplitudes for the motor phases which the IGBT switch circuitry implements. For running the sensor FOC, three feedback signals from 12-bit ADC inputs are needed. Two ADC inputs are used for reading the two-phase currents (Ia and Ib), and one channel is connected to measure the DC BUS voltage from where the motor is supplied.

The angle speed sensor data is connected through a serial peripheral interface, and one SPI is dedicated for this purpose. The CAN interface is used to communicate with the system MCPU. For the software upload and debugging, a JTAG interface is used. And for communicating with the ST motor control workbench, a serial interface is needed. An RS-232 transceiver is connected in one MCU UART port for this purpose.

The selected STM32F407VET microcontroller features 512 kB of Flash and 192 kB of RAM. The MCU is based on a Cortex-M4 32-bit RISC core, with an operating frequency of up to 168 MHz. The microcontroller has a floating-point unit and implements a full set of digital signal processing (DSP) instructions and a memory protection unit for enhanced application security.

The MCU has two advanced-control timers that are used as three-phase PWM generators, the resolution of the timers is 16 bit, and the modulation capability of the PWM output is 0-100 %. The timer outputs are multiplexed on six channels for driving the high and low side switches. The PWM generators have complementary outputs with programmable inserted dead-times. These high-resolution PWM timers are used to generate the drive signals for the IGBT module. The switching frequency of the PWM generator is fixed to 16 kHz.

The pin mapping and the configuration of the MCU were done with STM32CubeMX software. The CubeMX is a graphical tool for MCU selection, pin mapping, peripheral selection, and clock configuration.

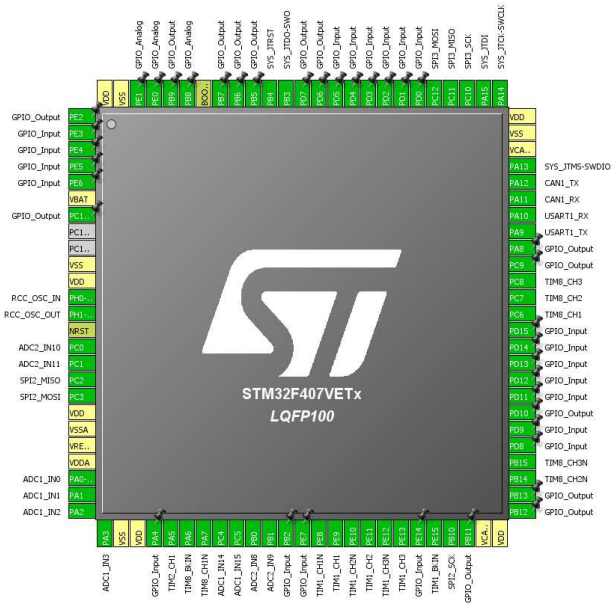

Figure 17. A STM32CubeMX graphical design view from the selected MCU pin mapping

After the pin mapping and configuration is done, the CubeMX can be used to create an initialization file for the MCU. The schematic symbol is drawn in PADS, based on the CubeMX model.

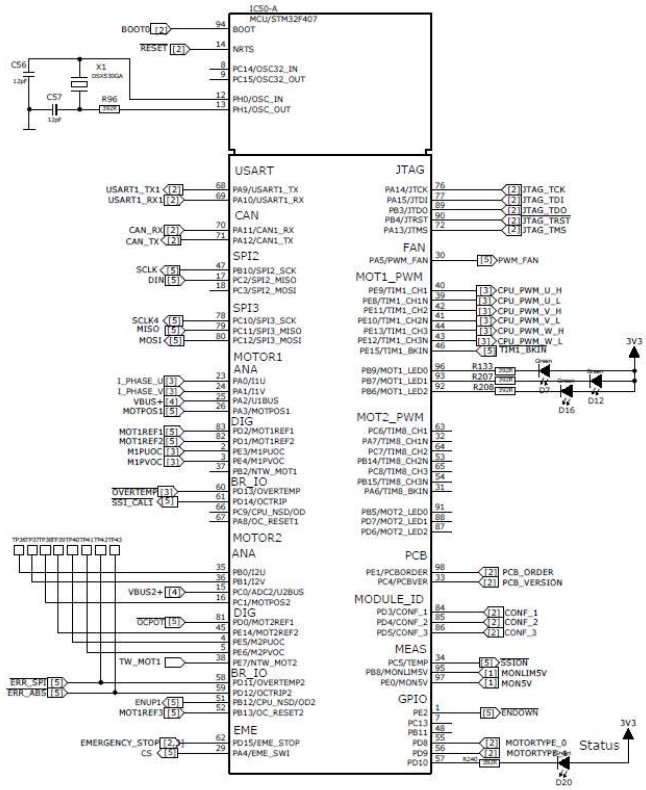

Figure 18. Schematic symbol of the MCU in PADS

The STM32CubeMX design is transferred into PADS manually. Also, the created schematic symbol is shown in Figure 18.

3.2.3 IGBT Module

The module power switching circuitry consists of three half-bridges, each consisting of a high and a low side switch with a high and low side driver. The high and low side switching is complementary. This means that when the switch is turned on, the other is turned off, with dead-time in between to prevent a shoot-through event that can result in a broken bridge.

The selected (STGIB10CH60TS-E) IGBT module features a 15 A, 600 V ~3 inverter bridge, with an integrated gate driving circuitry and freewheeling diodes. The selected module utilizes a short circuit rugged trench gate field-stop IGBTs, which are ideal to drives operating up to 20 kHz in hard-switching circuitries.

The interface between the microcontroller and the power stage is isolated with optocouplers for achieving the isolation requirement (Figure 19).

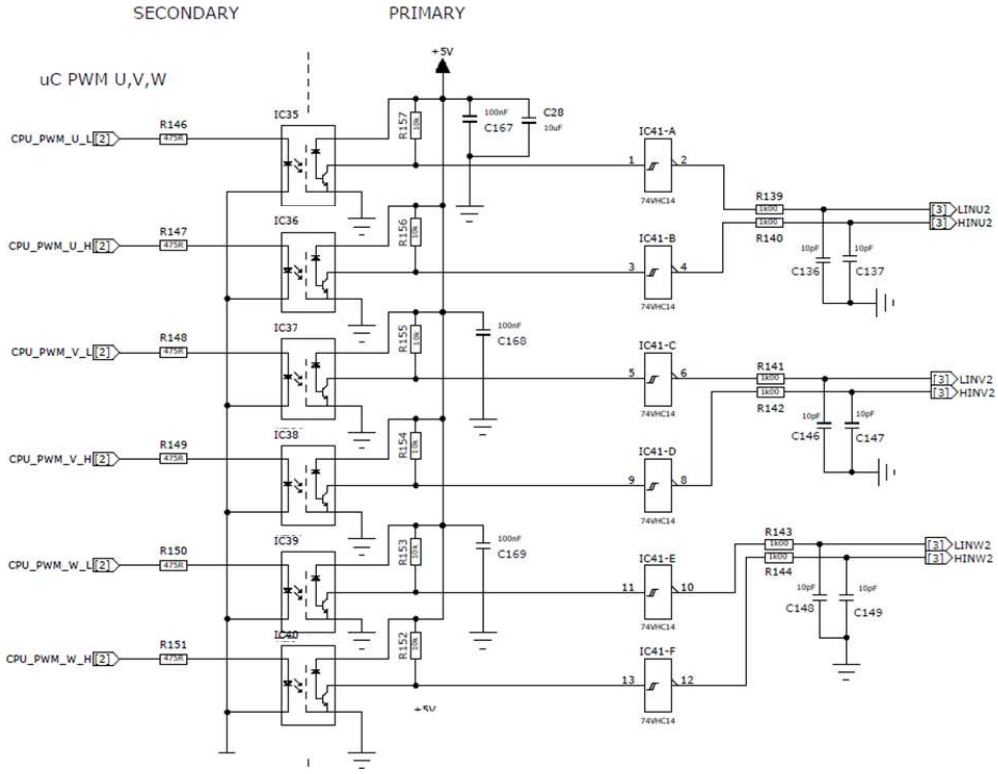

Figure 19. PWM optocoupler interface between MCU and IGBT module

The optocoupler provides double insulation between the secondary and the primary circuits. The PWM signals (HIN/LIN U, V, W) are conditioned with hex Schmitt inverter IC, which enhances the input signal into a sharp jitter-free output, which is then coupled into IGBT driver circuitry.

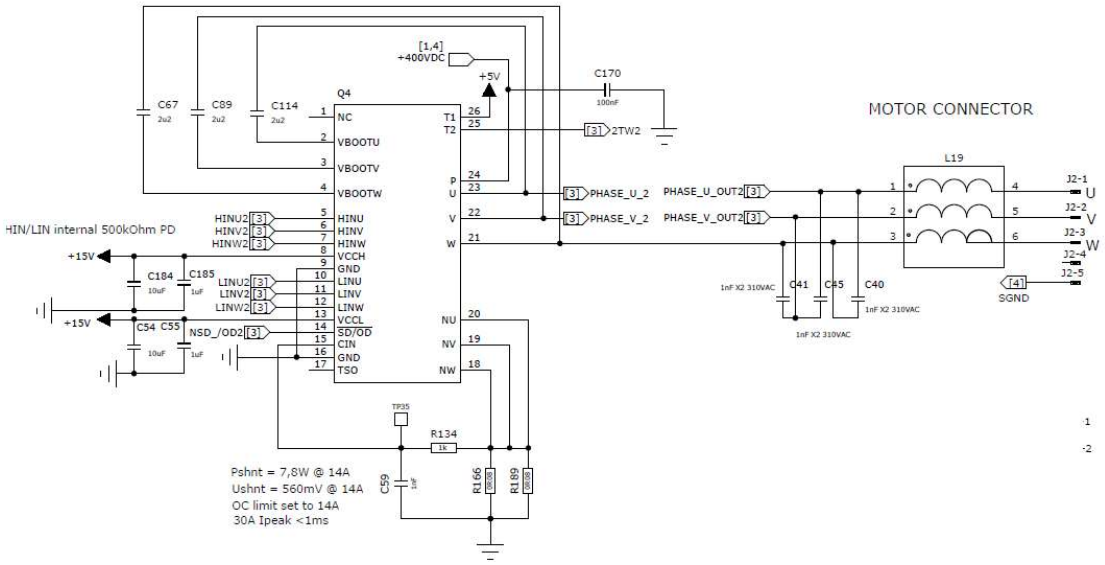

Figure 20. Power stage and motor connector

In Figure 20, each phase (U, V, W) has two PWM control signals connected from the microcontroller for high- and low-side switches. The IGBT module has a fast comparator for fault protection. And this is used for short circuit protection. The Cin pin is connected to measure the shunt voltage of R166 and R189 and is set to trip at 14 Amps, also having an RC time delay that can be configured with R134 and C59.

The IGBT has an NTC resistor connection on pins 25 and 26, and this is used for monitoring the module temperature. The temperature reading is transformed into binary data by using a non-inverting comparator with hysteresis that is set to trip at 125 C° and to recover at 111 C° — described in figure 21. The IGBT temperature data is forwarded to MCU, which can decide if the movement can be allowed to finish, before the cooling period.

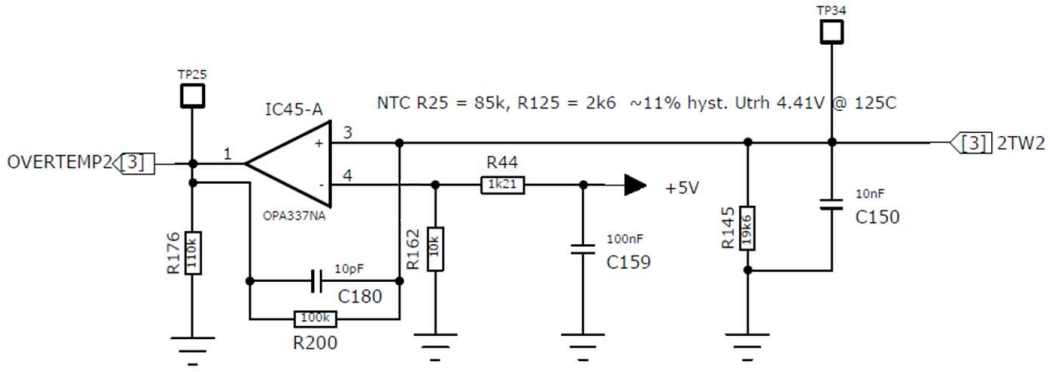

Figure 21. Temperature measurement comparator circuitry

The three-phase IGBT inverter bridge needs to deliver at least 500 W of power to the motor. The estimation of power loss in switching circuitry is calculated by adding all the energies that are dissipated in the switch. These state change energies (on-off), conduction losses, and reverse recovery energy are calculated and multiplied by the rate of switching.

The IGBT module provider offers a simulation tool for power loss estimation. So for simplicity, the ST Power studio, electro-thermal simulation software is used. Parameters for the simulations are presented in Figure 22. The 8 second corresponds to the application motor power consumption maximum. The heat sink is fixed, and the estimated thermal resistance R_{th} is 2 C°/ W.

Input Data

		Limits	
t_sim:	Simulation time (s)	0.001 ÷ 15	8.000
Iph:	RMS Phase Current (A)	0.01 ÷ 15	1.55
Pout:	Output Power (W)	0.1 ÷ 20000	503.07
Vdc:	DC Link Voltage (V)	20 ÷ 450	450.00
fsw:	Switching Frequency (kHz)	1 ÷ 40	16.0
fsine:	Output Frequency (Hz)	0.1 ÷ 500	75.00
PF:	Power Factor	0.1 ÷ 1	0.80
MI:	Modulation Index	0.01 ÷ 1	0.85
Tamb:	Ambient Temperature (°C)	25 ÷ 100	35.0

Output Data

	T1	D1
Conduction Loss (avg) (W)	0.54	0.15
Switching Loss (avg) (W)	0.93	0.08
Total Loss (avg) (W)	1.47	0.23
Junction Temp. (Max) (°C)	59.71	56.03
Junction Temp. (avg) (°C)	58.27	55.69
T1+D1 Total Loss (avg) (W)	1.70	
System Total Loss (avg) (W)	10.23	
Case Temp. (Max)(°C)	55.06	

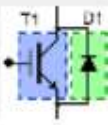

Figure 22. Simulator input and output data for power losses at 503 W load

The average power loss for the 8-second duration is 10.23 W resulting in a good efficiency coefficient. Only 2 % of input power is transformed into heat inside the power module. The Heat sink volume calculations can be found in Appendix 4.

Since the fast switching of IGBTs also generates electromagnetic interference, a filter with differential and common mode noise suppression stages is used to suppress the EMI. In Figure 20, The line-to-line X-capacitors (C40,41 and C45) act as a high frequency shunts for differential noise. And for suppressing a common mode noise, a three-phase common-mode-choke is used. The CMC (L19) utilizes a nanocrystalline core — trade name, Vitroperm, which has enhanced performance vs. traditional ferrite. Vitroperm cores provide high permeability characteristics enabling higher inductances with a lesser number of turns. This also minimizes the component size and improves high-frequency properties.

3.2.4 Voltage and Current Measurements

The DC-bus voltage and phase currents Ia and Ib are needed in order to execute the FOC algorithm successfully. The DC-bus voltage is measured with optically isolated voltage sensor ACPL-C87B, providing double insulation, described in figure 23. The differential output of the sensor is proportional to the voltage divider R206 / R115 voltage. The differential voltage is converted into a single-ended signal in an operational amplifier (OPA337NA) with a gain set by R79/R76. The output voltage from the differential to the single-ended amplifier is coupled to a 12 bit ADC of the MCU.

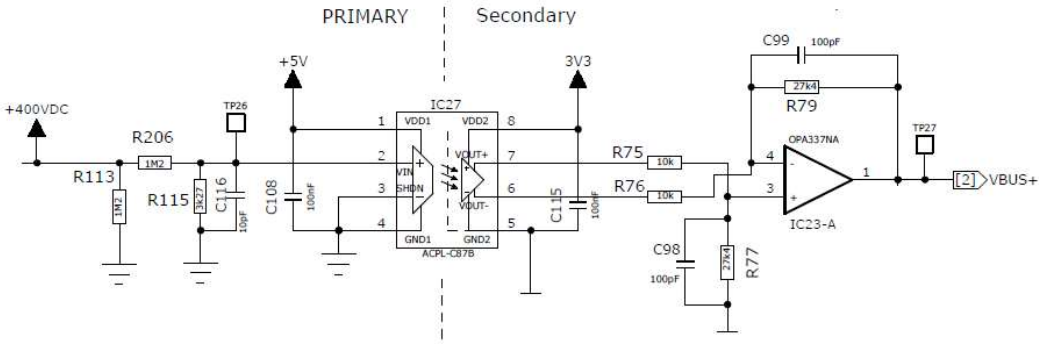

Figure 23. DC BUS optoisolated voltage measurement

Because the output common-mode rejection ratio (CMRR) of the differential to the single-ended configuration is impacted mostly by the accuracy of the resistors used in

R75,76,77 and R79, the resistors are specified into 1% tolerance. The selected operational amplifier OPA337NA has a bandwidth of 3 MHz and a slew rate of 1.2 V/µs.
The ACPL-C87B voltage sensor has a full-scale differential input range of 2.46 V. And an output voltage range of ±1.23 V. At the 450 VDC. The input voltage equals 1.222 V.

The input impedance of the voltage sensor (Vin) is > 1 GOhm, and it can be left remarked from the calculations as the ratio versus voltage divider resistor R115 is in a magnitude of parts per million (3.27×10^{-6}).

The ACPL-C87B has a differential voltage output of ±0.611 V at 450VDC input, and this voltage is to be converted to a single-ended signal through the differential to the single-ended amplifier.

For the current measurements, isolated current transducers manufactured by LEM are used. Two devices are configured for measuring the Ia and Ib currents. The control algorithm solves the Ic, as the balanced three-phase system vector sum of currents is zero.

The current sensing circuitry of the driver consists of a galvanically isolated current transducer. A signal amplifying and conditioning circuitry, consisting A rail-to-rail, high slew rate, and bandwidth (SR=6 V/µs and BW=5.5 MHz) operational amplifier and a low pass RC filter (Cut-off frequency = 338 kHz). In figure 24. current sensing schematic for phase U is presented.

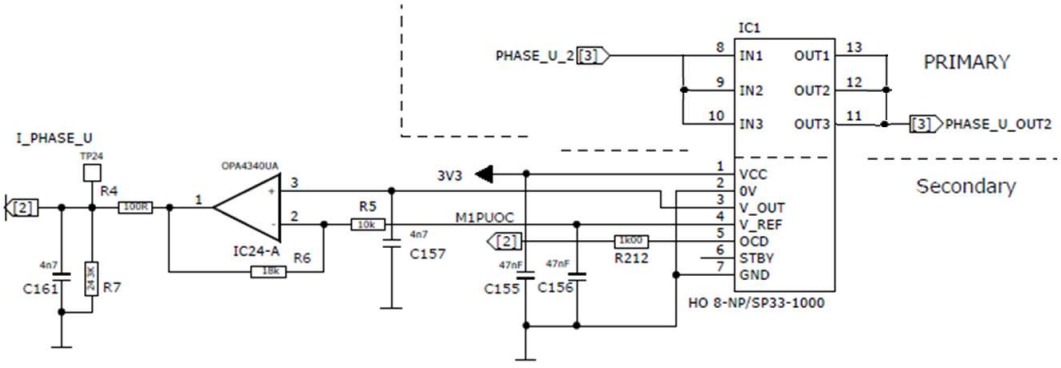

Figure 24. Current sensing circuitry

The current transducer is set to measure the primary current in 8 A nominal RMS current range with a total measuring range of -20 A to +20 A

The current transducer outputs a voltage proportional to the measured primary current. The V_OUT pin outputs in the primary zero-current condition a voltage of VCC/2. This equals that the zero current voltage is 1.65 V. Before the driver PWM generation, zero current initialization is conducted. Before the motor stator is powered, the zero current status is read from the ADC input and set as zero current. The negative currents are expressed as voltages <1.65 V (offset), and voltages >1.65 V is interpreted as positive currents.

3.2.5 Safety

The emergency stop signal is user-activated, and the optoisolator passes it into the power stage. The emergency stop signal forces the IGBT three-phase half-bridges into High-Z state and enables the brake. In a system-level, the emergency stop signaling is configured in such a way that a single fault condition, for example, a wire cut, is detected. The emergency switch is normally closed and provides the ground potential. When pressed, the internal pull-up resistor divider generates the signal to stop the power stage.

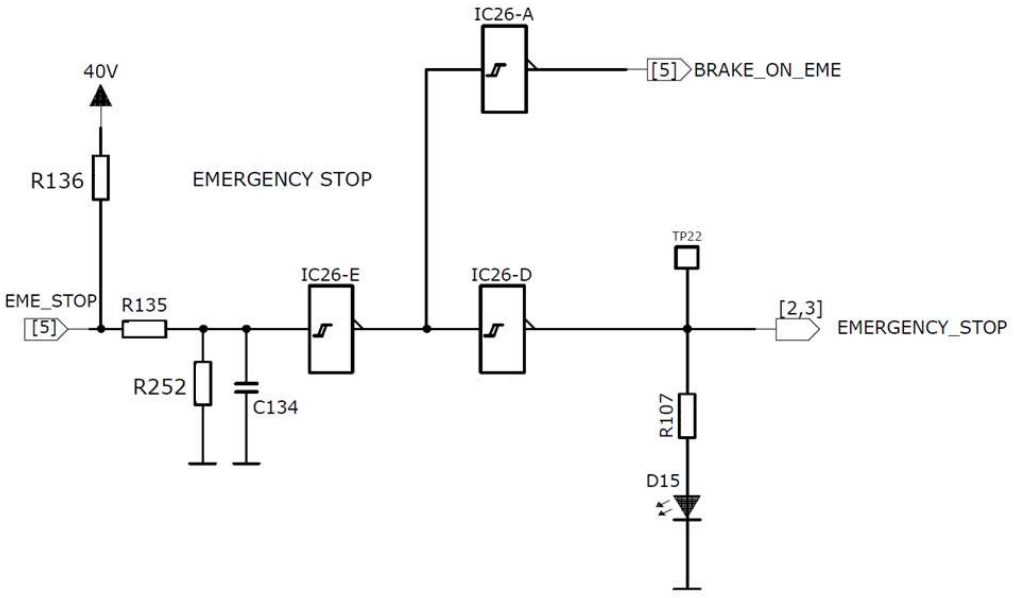

Figure 25. Emergency Stop circuit

The used 40 V signal level and R136, R135, C134 time constant with Schmitt trigger prevents transients enabling the emergency circuit. The signal is duplicated into CAN bus message.

3.2.6 ST Motor Control Workbench

The motor control software development kit allows evaluating the performance of the STM32 microcontroller in applications driving PMSM. The SDK introduces several tools for developing, such as motor profiler and motor control workbench. The PMSM FOC library is written in C language and implements the core motor control algorithms, such as reference frame transformations, current regulation, speed regulation, space vector modulation, and energy efficiency optimization.

In this study, the STM32 PMSM FOC software development kit version 4.3 is used to configure the hardware to run the PMSM, and Figure 26 presents the GUI of ST motor control workbench.

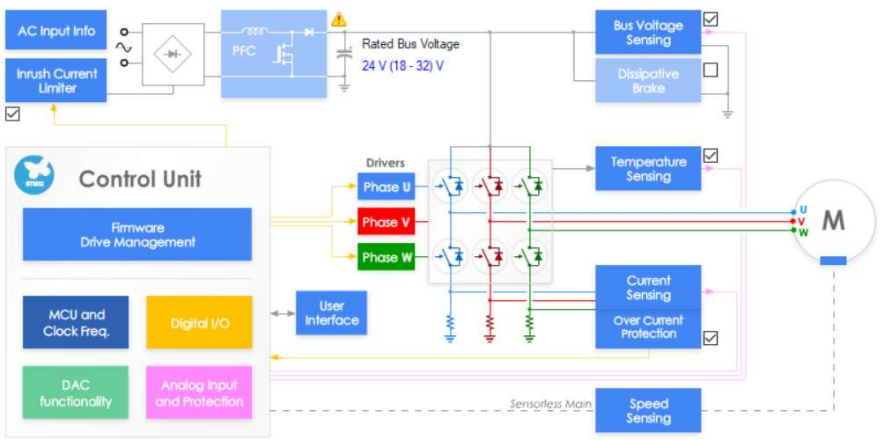

Figure 26 GUI screenshot from system setup of ST Motor Control Workbench

The application runs in PC and is connected to a driver through the serial interface. It can generate all the configuration files for the application, and from the GUI, a set of FOC variables can also be monitored and adjusted in real-time.

The ST motor Profiler tool can extract the electrical parameters from the motor. The motor profiler algorithm can solve the Stator resistance Rs, stator inductance Ls, B-EMF constant inertia, and friction. However, for some current reading topologies (ICs), the motor profiler lacks this support, so these need to be solved manually.

3.3 Rotor Speed Sensor

The sensor is used for motor rotor angular position and angular velocity measurement, by feeding a real-time rotor speed and angle data into a vector control algorithm.
The sensor type is TLE5012BE, and a custom PCB was designed for the system.

The sensor PCB utilizes a 4-wire SPI connection, but the TLE5012BE has a 3-wire SSC connection, which is SPI compatible. And since the SPI is not intended to be used over a long distance, and because of the sensor data reliability, the single-ended SPI is transformed into differential signals by using a dual RS-422 transceiver.

In figure 27. The sensor data in pin 4, is bi-directional, and in this case, when the differential driver is used, the direction is needed to control by the master device.

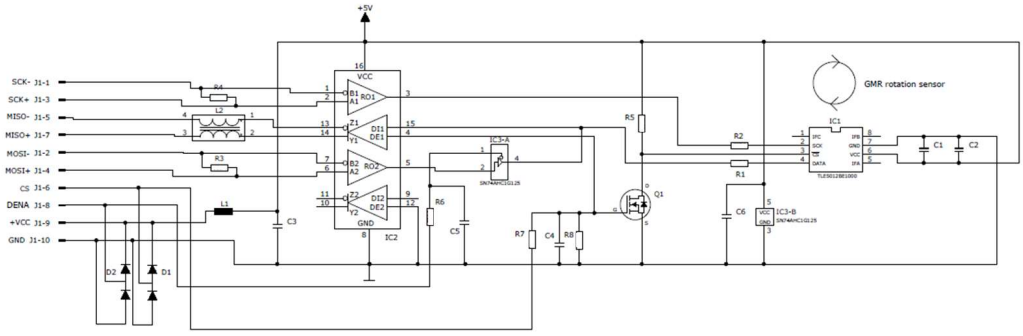

Figure 27. Speed sensor schematic

A data enable signal from the driver MCU (DENA) signal is used for changing the data direction.

4 Testing and Results

For testing the motion control performance, the first step was to test the custom driver hardware. The first patch of driver hardware was ordered from the PCB manufacturer and took three months from order to delivery. After the hardware was received, it was functionally tested.

4.1 Hardware Testing

The hardware testing was done by checking the PCB for short circuits with DMM and visually inspecting the component polarity, values, and solders. After precheck, the PCB was powered from the laboratory power source with a moderate current limit. The electronics were successfully powered, and no signs of heating of any component were observed with a thermal imager. A thermal imager would indicate the design or production flaws if any part or component would draw excess current and build up heat. For the buck and linear regulators, the voltage level, ripple voltage, supply current capability, and load step response measurements were done. Also, the emergency stop function was verified.

4.2 Software testing and parameter tuning

After the HW testing, the next step was to use the ST motor control workbench for creating a parameter header file for configuring the SW library for the driver MCU. The parameter header file includes all the variables for the FOC control algorithm to run successfully. These are the motor, power stage, drive management, and control stage-specific parameters. The workflow for generating the header file is described in figure 28.

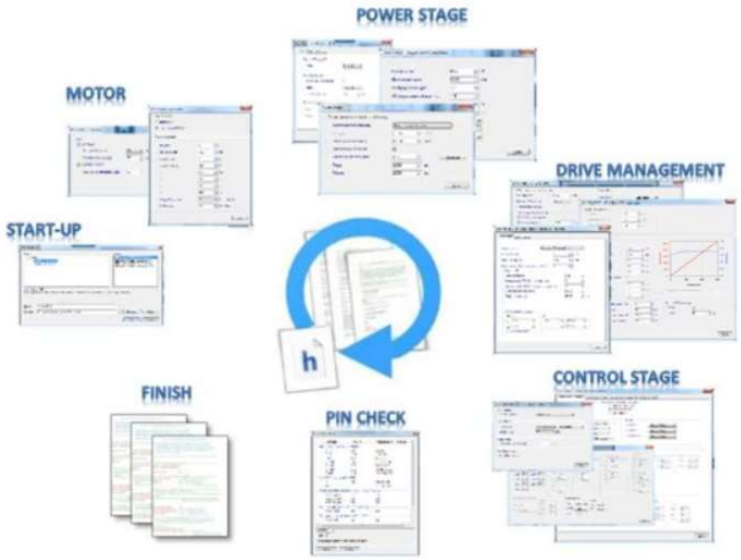

Figure 28. Building the header file in ST Motor control workbench (picture copied from ST motor control help file)

After feeding the required data for the header file creation, the next step was to compile and load the boot loader and the first software to MCU; this was done through the JTAG interface. The development SW included a serial interface for connecting to ST Motor control workbench. The motor control workbench was running in a laptop PC, and the connection was made through a USB-to-serial adapter. The driver has an RS-232 transceiver connected to the UART port for this purpose.

From the GUI in the ST motor control workbench, the connection setting was adjusted by selecting the correct COM port and baud rate for the connection.

When the driver connection and the ST motor control interface connection were established, the next step was to start the motor. And before the custom speed sensor was introduced for the motor controller. The motor testing was done in sensor-less mode.

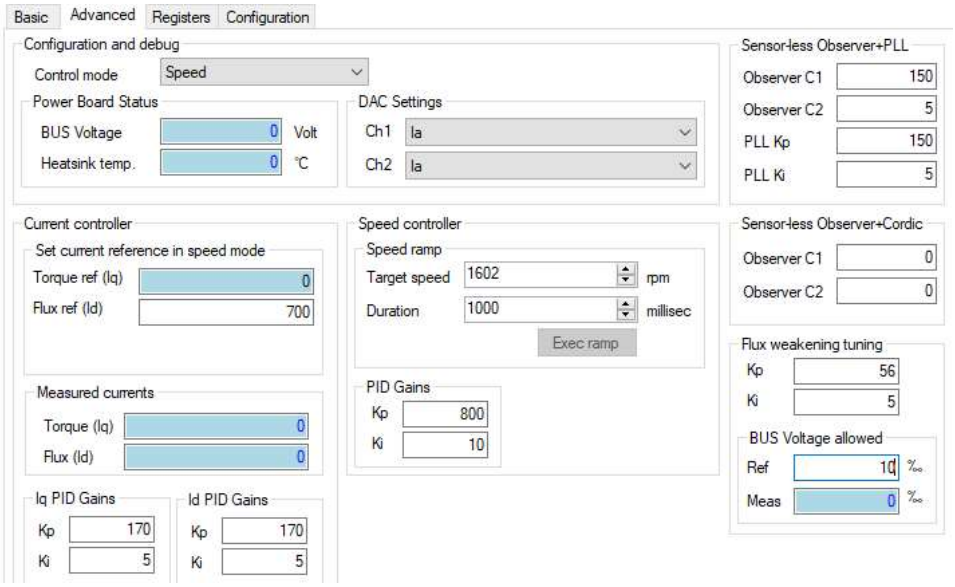

Figure 29. Configuring the Kp, Ki, and sensor-less Observer +PLL

In the MCU, there is support for two digital to analog converter output channels for printing the user-selected parameters from the FOC control. The DAC outputs are used for tuning the gains for torque and flux measurements and the sensor-less observer.

Before adjusting the torque and flux control, the DAC outputs were configured to print the Ia and Ib values for verifying the current measurements. An oscilloscope was connected to these channels, and two more oscilloscope channels were connected to measure the actual motor currents in phases U and V. The slight differences were compensated by adjusting the ICS current gain parameter in ST motor control workbench.

The next step was to fine-tune the observer parameters. The header file includes a raw estimation of parameters for the first spinning of the motor. For enhanced performance in lower motor speeds, the observer parameters are needed to tune.

For tuning the observer parameters, the observer back-electromotive force α and β were selected to be printed in DAC ports (Figure 30). The tuning was done by iterating the observer and phase-locked loop parameters.

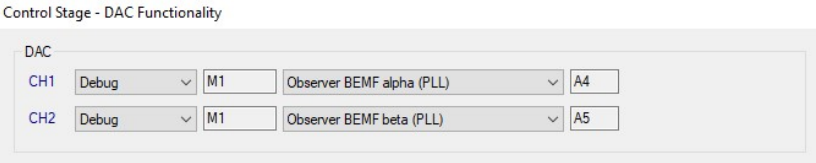

Figure 30. DAC output from the MCU setup

The goal for the tuning was that the BEMF signals would resemble the sine wave shape as much as possible. After the tuning, the lowest achieved rpm, where the motor was started and stayed in observer mode, was around 120 rpm. In the observer mode, the motor is started in an open-loop condition. The rpm threshold where the closed-loop control begins is configurable through the workbench interface.

When the motor parameters were verified in the test setup, the motor and the driver were assembled in the prototype device. The motor performance was tested with various load configurations in gantry mechanics, the rpm consistency was observed through the absolute encoder readings and from the speed plotting tool available in the ST motor control interface.

When the mechanics and drive system were verified, the next step was to connect the custom speed sensor to motor chassis and feed the speed data from the sensor into the correct phase of the FOC control loop (Figure 31). With the use of a rotor position and speed sensor, the drive system was able to achieve the full rpm range from 0 rpm to 6000 rpm. The software modification was not done by the author.

Figure 31. Rotor speed sensor mounted in motor chassis

The speed sensor PCB is mounted into a motor frame and is observing the magnet that is fixed into the rotor shaft. The sensor detects the orientation of the magnetic field and outputs the angle measurement. The sensor has an internal revolution counter and can output the needed angle speed into the FOC algorithm.

The sensor is positioned at a 90° electrical angle by applying a DC voltage to motor coils. The rotor positions regarding the magnetized coils by turning and locking the rotor and the magnet into a fixed position. A software tool is then used to read the sensor angle, and the PCB is rotated to align the magnetic field with the sensor reading. When the electrical desired angle is found, the sensor is secured with four screws and a marking.

When the motor driver was running in sensor mode, the next phase was to build the communication protocol with the MCPU through CAN bus. After the connection, the system was as it is described in motion control system architecture in figure 13. Now the system was ready for performance testing of the motion control.

4.3 Performance testing

For analyzing how well the system is performing a test setup was defined for the prototype device. For the test setup, the MCPU has been configured to output the calculated angle difference between the plotted position and the actual position measured by the absolute position encoder. The limits for allowable angle difference was calculated, from the positioning accuracy specified in the requirements specification. The acquired data from MCPU was passed through an ethernet connection into PC, where a data plotting tool was used for generating a visual presentation of data. The tool that was used is Matplotlib, which is a Python 2D plotting library that produces figures which can be used in Python scripts.

The performance testing was done in the actual CBCT device prototype by using the worst-case scenario, where the motion control system would need to deliver the maximum power and speed in unbalanced load conditions. This was an 8-second revolution with acceleration and deceleration with a maximum of 6800 rpm.

In the prototype CBCT device, the length of the outer edge of the rotating gantry is 400 cm, and it is where the angle difference is measured. The drive system performance is described in figure 30. presenting a plotted graph from the CBCT device, when rotated 460°, and the gantry was unbalanced with dumbbell weights.

The specified accuracy from the requirement specification regarding the positioning was ±150 µm. This accuracy is measured from the maximum acquired 3D volumes outer surface. The volume diameter is 215 mm. The corresponding angle (α) is calculated simply by solving the equations 1 and 2.

$$\frac{215\ mm * \pi}{360°} * \alpha = 150\ \mu m \tag{1}$$

$$\frac{1}{\alpha} = \frac{215mm * \pi}{360°} \tag{2}$$

α =0.0799° ~ **±0.08**°

So the angle α is the angle difference allowed on drive positioning accuracy during exposure with sensor reading accuracy and is marked with red lines windowing the area where the gantry position is allowed to drift during the image acquisition.

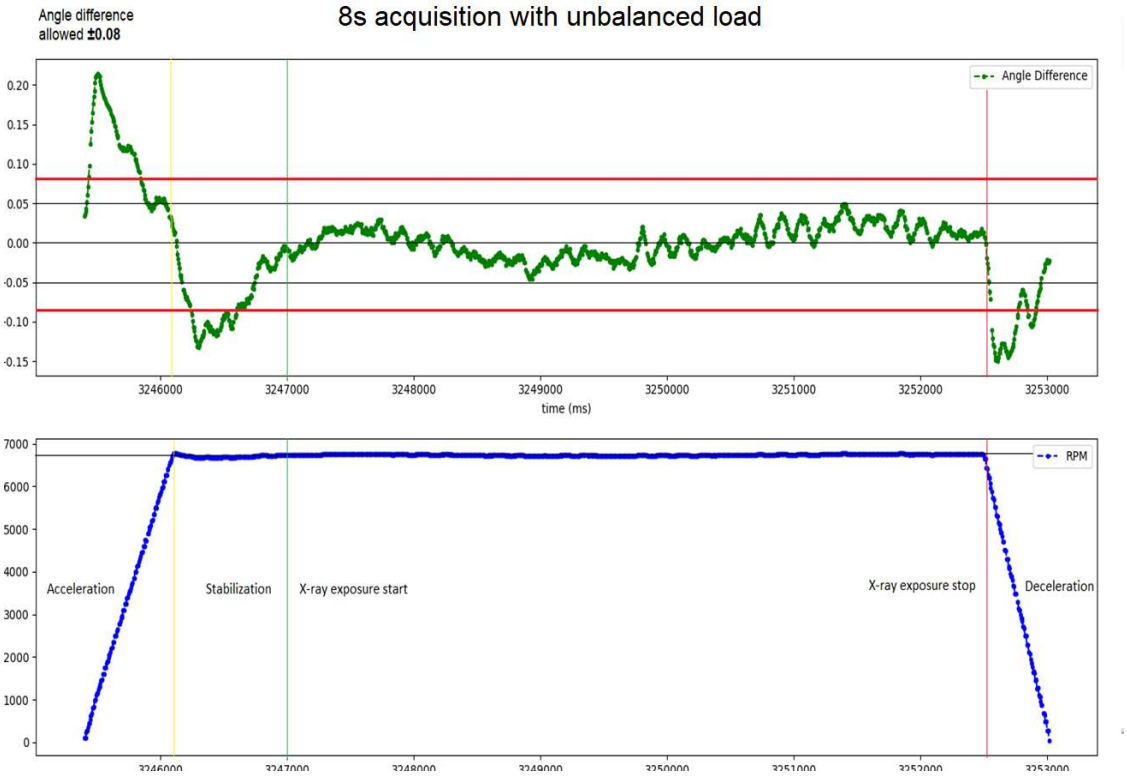

Figure 32. The performance of the motion controller with allowable (RED) limits and acquisition sequence

The green plotted graph in figure 32. presents the difference error from the measured absolute encoder position vs. setpoint from the MCPU. The drive sequence is divided into four phases, and these are 1. Accelerating, 2. Stabilization 3. Image acquisition, and 4. Deceleration. The stabilization stage is used in a trapezoidal speed profile. And the positioning is allowed to differ more in the acceleration phase than in the image acquisition phase.

4.4 Results

From the plotted graph (figure 32), the maximum 0.05-degree difference error in gantry outer edge means that the actual distance (d_α) between gantry position and guide value during the exposure is:

$$d\alpha = \frac{400\ cm}{360^\circ} * 0{,}05^\circ = 0{,}55\ \text{mm} \quad (3)$$

This means that the imaging devices are positioned at their rotational path inside ±0,55 mm, from the MCPU position plot in any given time at the image acquisition phase.

The positioning accuracy is then transferred at the volume geometry, which has a diameter of 21.5 cm. The distance dα positioned on volume surface (dα2) translates:

$$d\alpha 2 = \frac{215\ \text{mm} * \pi}{360^\circ} * 0{,}05^\circ = 0{,}094\ \text{mm} \quad (4)$$

This means that in the acquired CBCT 3D volume, the achieved positioning accuracy during exposure is, ±94 μm. This measured value is less than the specified ±150 μm position accuracy from the requirement specification.

5 Conclusions and Discussion

The selected drive system and motion control performed well in the performance test phase. The positioning accuracy achieved during the 8 s scan time was ±0.05, [limit ±0.08°].

The motion control design for the prototype device described in this study fulfills the requirement specification, so the goal for this study was achieved.

During the testing with different loads and trajectories, some indications emerged that the motor lacked some torque. In the future, if more weight is added into gantry construction, a motor with a higher torque should be considered.

After a brief discussion with the motor manufacturer, it was possible to get a 50 % increase in the torque by mounting a longer rotor and windings into the same motor frame. This also enabled the increase of the tooth count in the primary driving tooth wheel and adjusted the maximum needed rpm close to the motor nominal speed. This modification also decreases the voltage amplitudes during the electric braking mode.

The overall image quality and achievable spatial resolution of an X-ray system are dependent on several factors. Mainly the X-ray source performance, source to image distance, image detector quality, dose, calibrations, and the use of correction and reconstruction algorithms. The part where the motion control contributes to the image X-ray image quality is the consistency of the motion and to produce a vibration-free imaging device. The vibration and inconsistency of movement creates a movement and ring artifact, degrades the geometry calibration, and can be observed in acquired raw data or reconstructed 3D volume. The motion control-related artifacts should be avoided in CBCT imaging.

A closed-loop control system is mandatory by the basis of positioning accuracy requirement, which was set to be ≤ 150 µm measured from the surface of the maximum volume. The tuning of the controller is needed to avoid causing stimulus for mechanical vibrations, and especially using S-curves in trajectory plots for minimizing mechanical jerks. In this study, a trapezoidal rpm profile was used, and though it performed admirably. It was replaced later with the S-curve profile.

References

1. Planmeca Group, [Online] Available: https://www.planmeca.com/company/planmeca-group/ [Accessed 13 October 2019]
2. X-ray Imaging [Online] Available: http://bme.elektro.dtu.dk/31545/notes/ct_reconstruction_ver_2016_2_slides.pdf [Accessed 13 October 2019]
3. Schleifring, CT construction and slipring [Online] Available: https://docplayer.net/43250721-Slip-ring-solutions-ct-applications.html [Accessed 13 October 2019]
4. Recent and future directions of CT imaging [Online] Available: https://www.ncbi.nlm.nih.gov/pmc/articles/PMC3958932/ [Accessed 13 October 2019]
5. Hakan Gürocak, Industrial motion control: Motor Selection, Drives, Controller Tuning, Applications, Wiley 2016
6. Mathworks, “what is feedforward control” [Online] Available: https://www.mathworks.com/videos/control-systems-in-practice-part-3-what-is-feedforward-control-1535712796292.html [Accessed 13 October 2019]
7. MachineDesign “What´s the difference between AC induction, Permanent magnet and servomotor technologies” [Online] Available: https://www.machinedesign.com/motorsdrives/whats-difference-between-ac-induction-permanent-magnet-and-servomotor-technologies [Accessed 13 October 2019]
8. Texas instruments, Motor control compendium [Online] Available: http://www.ti.com/download/trng/docs/c2000/TI_MotorControlCompendium_2010.pdf [Accessed 13 October 2019]
9. Power Electronics “The case for the switched reluctance motors” [Online] Available: https://www.powerelectronics.com/content/case-switched-reluctance-motors [Accessed 13 October 2019]
10. Electronic Design, “IGBTs Or MOSFETs: which is better for your design” [Online] Available: https://www.electronicdesign.com/power/igbts-or-mosfets-which-better-your-design [Accessed 13 October 2019]
11. NXP, “Sensorless PMSM Field-Oriented Control” [Online] Available: http://cache.freescale.com/files/microcontrollers/doc/ref_manual/DRM148.pdf [Accessed 13 October 2019]

12. National instruments, “Three-Phase Inverter” [Online] Available: http://zone.ni.com/reference/en-XX/help/374169C-01/lvemsimshared/inverter/ Inverter [Accessed 13 October 2019]
13. A Practical Primer On Motor Drives (Part 13): Motor Drive Control Architectures and Algorithms” [Online] Available: http://www.how2power.com/pdf_view.php?url=/newsletters/1702/articles/H2PToday1702_design_TeledyneLeCroy_part13.pdf [Accessed 13 October 2019]
14. Switchcraft, “Vector Control For Dummies” [Online] Available:https://www.switchcraft.org/learning/2016/12/16/vector-control-for-dummies [Accessed 13 October 2019]
15. semanticscholar.org, “Direct Torque Control of Induction Motor With Improved Switching Scheme” [Online] Available: https://pdfs.semanticscholar.org/8c8e/1c659b29fedb414931e87b74eae6caae045b.pdf [Accessed 13 October 2019]

Requirements specification, project XFI

XFI-363 - Duty cycle and performance - rotation movement
Duty cycle:

- Actions per duty cycle
    - Entry position -> start position
    - 360 rotation
    - Back to the entry position
- Worst case duty cycle: 2x end-to-end movement per image acquisition

End-to-end movement speed requirement:

- Acceleration ramp: 2s
- Imaging / 360degree rotation: 7s (8s - marginal between "hengittämättä" command and start of imaging)
- Deceleration: not relevant as long as movement range allows (90 degrees reserved for acceleration + deceleration)

Positioning accuracy:

- +/- 0.15mm (one pixel)
- Absolute position sensor required

Priority Medium [50.0]
XFI-435 - Rotation motor duty cycle
Duty cycle at least 1:20
Continuous movement at least 14s
Priority Medium [50.0]
XFI-436 - Rotation movement accuracy
Rotation movement track highly repeatable
- Focal spot and detector position repeatable to <1mm from the rotation - to - rotation.
Priority Medium [50.0]
XFI-437 - Rotation positioning sensor
- Absolute positioning sensor with accuracy and repeatability less than 0.15mm.

Driver specification

The Motor driver PCB specification:

- Gantry movement
- Microcontroller STM32F407 100-pin LQFP
- Critical components need to be UL-listed, E-file
- Power stage IGBT module
- Heatsink thermal design should allow the worst-case duty cycle
- Generate and regulate the voltages needed for driver and control circuitry
- Primary, secondary dual insulation
- To receive positioning orders via CAN bus from the MCPU
- Possibility to continue the cabling
- DC input EMI filtering
- Motor output du/dt filter
- Isolating current and DC BUS voltage measurement
- Voltage and status LED indicators
- Identification coding, motor type, driver version, PCB version, and order
- Connections
    - DC BUS 450VDC Primary
    - DC 40VDC Secondary
    - JTAG -connector
    - RS-232 Serial interface
    - Absolute encoders are measuring the movement. SSI and VCC
    - Limit switch interface 2 / movement
    - Rotor position and angle speed sensor connection SPI
    - CAN 2.0b and selectable termination configuration
    - Motor thermal switch NTC
    - Emergency switch
    - Safety line
    - Pass through EXP ind / Switch signals
    - Motor output UVW,
    - Motor cable shielding PE connection
    - brake / fan connection

- Schematic and design shall follow the inhouse electronics design guideline and DFT rules.

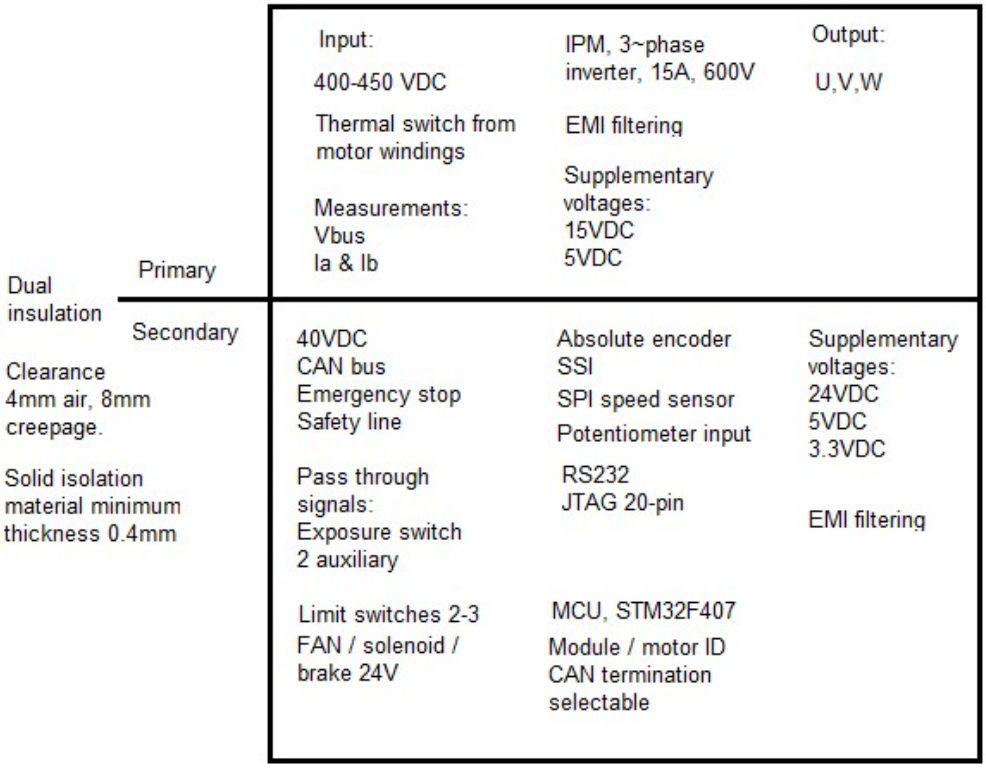

Motor parameters of S56

Rated Motor Parameters for S56

Rated Voltage	= 200,0 V
Rated Current	= 2,00 A
Rated Speed	= 4500 U/min
No. of Pole Pairs	= 1
Rated Frequency	= 75,00 Hz
Rated Mech. Power	= 0,5 kW

Additional Motor Parameters

Voltage Constant	= 26,0 mVmin
Stator Inductance	= 94,9 mH
Stator Resistance	= 58,345 Ohm
Peak Current	= 6,70 A

Heatsink volume calculation

V= (Q*Rv)/Delta T

Heat sink volume in cm^3 = (heat source power in watts x volumetric thermal resistance) / (Tjunction - maximum ambient temperature)

Inputs (in yellow)

Heat Source Power (Q)	15.0	Watt
Tcase Max (manuf supplied)	125.0	Deg. C
Max Ambient Temperature	60.0	Deg. C
Delta - T (Thermal Budget)	65.0	Deg. C
Volumetric Thermal Resistance (Rv) *(refer to table at right)*	150.0	
Estimated Heat Sink Volume	**34.6**	**cm^3**

Air Flow	Properties	Volumetric Thermal Resistance
Natural Convection	Little to no air / no noise	Rv = 500 - 800
1.0 m/s ~200 lfm	Gentle air, very low noise	Rv = 150 - 250
2.5 m/s ~500 lfm	Moderate air	Rv = 80 - 150
5.0 m/s ~1,000 lfm	Fast, loud air	Rv = 50 - 80

1. Smaller heat sinks of 100-200 cm^3 use values in the lower Rv range.
2. Larger heat sinks of 1,000 cm^3 use values in the upper RV range.
3. Actual thermal resistance values may vary outside range based on several factors.
4. Model assumes fin design is optimized for a given air flow.

Desired Heat Sink Volume

Length	7.0	cm
Width	3.5	cm
Height (base plus fin)	3.0	cm
Desired Heat Sink Volume	**73.5**	**cm^3**

Your Desired Heat Sink Size is	**38.9**	**cm3 bigger than require**